American College of
Neuropsychopharmacology

ARTICLE

Check for updates

Structure and function differences in the prelimbic cortex to basolateral amygdala circuit mediate trait vulnerability in a novel model of acute social defeat stress in male mice

Yael S. Grossman[1,2], Clementine Fillinger[1], Alessia Manganaro[1,3], George Voren[1], Rachel Waldman[1], Tiffany Zou[1], William G. Janssen[1], Paul J. Kenny [1,4] and Dani Dumitriu [1,3,4,5,6,7,8,9,10,11,12 ✉]

Stressful life events are ubiquitous and well-known to negatively impact mental health. However, in both humans and animal models, there is large individual variability in how individuals respond to stress, with some but not all experiencing long-term adverse consequences. While there is growing understanding of the neurobiological underpinnings of the stress response, much less is known about how neurocircuits shaped by lifetime experiences are activated during an initial stressor and contribute to this selective vulnerability versus resilience. We developed a model of acute social defeat stress (ASDS) that allows classification of male mice into "susceptible" (socially avoidant) versus "resilient" (expressing control-level social approach) one hour after exposure to six minutes of social stress. Using circuit tracing and high-resolution confocal imaging, we explored differences in activation and dendritic spine density and morphology in the prelimbic cortex to basolateral amygdala (PL→BLA) circuit in resilient versus susceptible mice. Susceptible mice had greater PL→BLA recruitment during ASDS and activated PL→BLA neurons from susceptible mice had more and larger mushroom spines compared to resilient mice. We hypothesized identified structure/function differences indicate an overactive PL→BLA response in susceptible mice and used an intersectional chemogenetic approach to inhibit the PL→BLA circuit during or prior to ASDS. We found in both cases that this blocked ASDS-induced social avoidance. Overall, we show PL→BLA structure/function differences mediate divergent behavioral responses to ASDS in male mice. These results support PL→BLA circuit overactivity during stress as a biomarker of trait vulnerability and potential target for prevention of stress-induced psychopathology.

INTRODUCTION

Stressful events are common causes of psychopathology, including major depressive disorder, the disease accounting for most years with disability worldwide [1]. However, irrespective of the type, strength or duration of a stressor, significant individual variability exists in stress-responses. Several preexisting traits, features of cognitive development, and environmental factors have been implicated in conferring resilience or vulnerability [2–9]. Identifying the vulnerable population could facilitate development of novel therapeutics, with the potential for alleviating [10], delaying [11], or preventing stress-induced disorders in at-risk individuals [12].

Chronic social defeat stress (CSDS) is a mouse model that has been well-validated for depressive and anxiety-like behaviors and reproducible classification of two distinct stress-induced phenotypes [13, 14]. Following CSDS, approximately two-thirds of experimental mice exhibit susceptible behavior, defined as acquired social avoidance, while one-third exhibit resilient behavior, defined as persistent social approach, similar to control mice. Accumulating evidence points to vast differences in numerous neurocircuits in resilient versus susceptible mice following CSDS [15]. However, much less is known about how the neurocircuits activated during a first-time stressor mediate downstream divergent stress-responses and circuit plasticity.

The prelimbic cortex to basolateral amygdala (PL→BLA) circuit is necessary for the acquisition of fear memory [16–18], involved in anxiety-like behavior [16, 19–22], and overactive in depressed patients [5, 23–28]. Furthermore, PL neurons have stunted dendritic arbors after CSDS [15, 29–31]. Therefore, differences in the function and structure of the PL→BLA circuit are good

[1]Department of Neuroscience, Icahn School of Medicine at Mount Sinai, New York, NY, USA. [2]Department of Psychiatry, Duke University School of Medicine, Durham, NC, USA. [3]Department of Pediatrics, Columbia University Irving Medical Center, New York, NY, USA. [4]Friedman Brain Institute, Icahn School of Medicine at Mount Sinai, New York, NY, USA. [5]Department of Pediatrics, Icahn School of Medicine at Mount Sinai, New York, NY, USA. [6]Department of Environmental Medicine & Public Health, Icahn School of Medicine at Mount Sinai, New York, NY, USA. [7]Mindich Child Health and Development Institute, Icahn School of Medicine at Mount Sinai, New York, NY, USA. [8]Department of Psychiatry, Columbia University Irving Medical Center, New York, NY, USA. [9]New York State Psychiatric Institute, Columbia University, New York, NY, USA. [10]Sackler Institute, Columbia University, New York, NY, USA. [11]Columbia Population Research Center, Columbia University, New York, NY, USA. [12]Zuckerman Institute, Columbia University, New York, NY, USA. ✉email: dani.dumitriu@columbia.edu

candidates for investigating mechanisms underlying divergent stress-responses.

We developed a model of acute social defeat stress (ASDS) that allows for rapid classification of susceptible and resilient mice, enabling mechanistic dissection of stress-activated PL→BLA neuronal structure/function differences and their contribution to divergent stress responses. Using tract-tracing in conjunction with the transcriptional activity marker cFos [32, 33], we show that mice susceptible to ASDS have greater proportion of stress-activated PL→BLA neurons compared to resilient mice. Furthermore, stress-activated PL→BLA neurons are morphologically different in susceptible versus resilient mice. Using an intersectional chemogenic approach, we then show both acute and chronic inhibition of this circuit blocks stress-induced social avoidance. Together, these results implicate PL→BLA overactivation as a biomarker of trait vulnerability and a promising target for prevention of stress-induced maladaptive behavior.

METHODS
See Extended methods in Supplementary Materials for detailed methods.

Animals
Experimental mice were 7–12-week-old C57BL/6J male mice, group-housed (4mice/cage), maintained on a 12-hour light/dark cycle (lights on 07:00), with ad libitum food and water. Retired breeder CD1 male mice displaying high levels of aggression during screening were used in social defeat experiments and non-aggressive male CD1 mice were used in social interaction (SI) testing. All experiments were conducted during the light cycle in compliance with National Institutes of Health Guidelines for Care and Use of Experimental Animals approved by Institutional Animal Care and Use Committee at Icahn School of Medicine at Mount Sinai.

Chronic social defeat stress (CSDS)
CSDS was performed as previously described [13, 14, 34]. Experimental mice were placed into cages of aggressive CD1 mice for 5 min/day for 10 consecutive days, thereafter remaining co-housed ~24 h with a clear perforated plexiglass partition prohibiting further aggression. Control mice interacted and were co-housed with non-aggressive con-specific mice daily. On day 10, experimental mice were singly-housed, then tested on SI on day 11.

Subthreshold social defeat stress (StSDS)
StSDS is a submaximal stressor not normally associated with social avoidance and used for assessing increased susceptibility in response to various manipulations [13, 14]. Experimental mice were placed into cages of three aggressive CD1 mice for 5 min each, with 15 min rest in a clean cage between sessions. Control mice were placed into cages of three non-aggressive conspecific mice. Experimental and control mice were then returned to group-housing with prior cage-mates and tested on SI 24 h later.

Acute social defeat stress (ASDS)
Various forms of acute social stress have been described [35–38], but an ASDS protocol resulting in divergent responses similar to CSDS has not previously been validated to the best of our knowledge. Experimental mice were placed into the cages of three aggressive CD1 mice for 2 min each sequentially, without rest periods. Control mice were placed into cages of three non-aggressive conspecific mice for 2 min each sequentially. All mice were then singly-housed in a clean cage for 54 min, then tested on SI. Immediately after SI, mice were either sacrificed or returned to group-housing with original cage-mates.

Key differences between StSDS and ASDS include rest periods versus consecutive aggressive bouts, co-housing versus single-housing following social defeat stress, and SI testing 24 h versus 54 min following stress. While these two tests likely activate similar neurocircuitry, ASDS was specifically developed for divergent stress-responses at a timepoint of maximal cFos expression, which StSDS has not been used for. StSDS was included here as a previously validated submaximal stressor to test stress-priming effects [13, 14]. See Extended Methods for further discussion.

Behavioral assays
SI was tested identically for CSDS, StSDS and ASDS. Experimental mice were placed into an opaque Plexiglas open-field arena (42 cm × 42 cm × 42 cm) with a removable wire-mesh enclosure placed against the middle of an inner wall of the arena. Mice first explored the arena for 150 s with "no target" present, then explored for 150 s with a novel non-aggressive CD1 "target" mouse in the enclosure. Video-tracking (Ethovision 3.0, Noldus Information Technology) was used to record movements. Total time spent in "interaction zone" (8 cm area surrounding enclosure) and "corner zones" (9 cm × 9 cm corners on opposite wall from enclosure) were quantified. Interaction and corner ratios were calculated by dividing time spent in respective zone during "target present" by time during "no target".

Classification into susceptible versus resilient
For experiments validating ASDS, "resilience" was defined as SI ratio ≥ 1 and "susceptibility" was defined as SI ratio < 1 in accordance with conventional classification [13] to allow for meaningful comparison to the substantial literature on CSDS. For experiments looking at PL→BLA activation and dendritic spine structure, a multidimensional more stringent classifier for resilience and susceptibility was used. These criteria were designed for three reasons. First, they exclude the weakly avoidant or socially "indifferent" behavior observed in a subset of both control and defeated mice. Second, using this classification system on ASDS-defeated mice has high sensitivity (83%) and specificity (59%) for mice that are resilient to the initial ASDS and remain resilient to a subsequent CSDS, indicating that using a multidimensional classifier taps into a more homogenous trait-resilient phenotype. Third, increased behavioral homogeneity improves identification of small effect sizes; this was crucial, as we hypothesized putative functional and structural differences to be very small given that they represent individual variability within a naïve population.

The following criteria were used to enhance the homogeneity of behavioral groups: First, all animals with an average velocity less than 1.8 cm/s were excluded. This population reflects 7.5% ($N = 27$ of 359) of defeated mice with "freezing" rather than avoidant behavior. This behavior is exceedingly rare in control mice (1.3%, $N = 2$ of 149). Because these mice can freeze anywhere within the arena when a target mouse is present, they occasionally freeze at the edge of the interaction zone leading to an artificially elevated SI ratio. In the PL→BLA activation and dendritic spine structure study, this population reflected 2.2% of defeated mice ($N = 1$ of 46). Resilience was then defined as meeting all three of the following criteria: SI ≥ 1, absolute time interacting with novel target mouse ≥60 s, and absolute time spent in corners when novel target mouse present <30 s. Susceptibility was defined as requiring both of the following criteria: SI ratio < 0.6 and absolute time spent interacting with target mouse <50 s. In our combined 17 experiments establishing the ASDS protocol, 68% ($N = 101$ of 149) of control mice met the resilience criteria and only 5.4% ($N = 8$ of 149) met the susceptibly criteria. In contrast, if a simple SI ratio below 1 is used to classify susceptibility, 24% of control mice ($N = 35$ of 149) would meet susceptibility criteria. Similarly, in the PL→BLA activation and structure study, 88% ($N = 13$ of 16) of controls met resilience criteria and only 7% ($N = 1$ of 16) met susceptibility criteria. These criteria are therefore useful for capturing the effects of social defeat without the confounder of weakly avoidant or socially indifferent mice.

Other behavioral testing
Using this multidimensional classifier, resilience represents 26% ($N = 92$ of 359) of the defeated population in our combined 17 experiments establishing the ASDS protocol, and 17% ($N = 8$ of 46) of the defeated population in the three experiments examining PL→BLA activation and morphological differences. Susceptible animals represent 32% ($N = 115$ of 359) and 46% ($N = 21$ of 46) in these populations respectively. Because the PL→BLA activation and structure difference experiment also required animals to have adequate stereotactic injections targeting the BLA and there were only eight resilient mice, one exception was made: one mouse meeting only two of the three criteria (absolute time interacting with novel target mouse and corner time) for resilience and had proper targeting of the BLA was included in the resilient group. In total, seven mice per group (control, resilient, susceptible) fit these criteria, had adequate targeting of the BLA, and were therefore included in post-hoc analyses.

For sucrose preference testing, mice were individually housed to quantify consumed fluids, underwent 2-day habituation to drink water

from two 50 mL conicals with sipper stops, then the content of one conical was replaced with 1% sucrose in water and fluid consumed from each conical was recorded at the end of 24 h. In open field testing (OFT), mice explored an empty opaque Plexiglas arena (42 cm × 42 cm × 42 cm) for 5 min and time spent in center (10 cm × 10 cm) was quantified using video-tracking. In elevated plus-maze (EPM) testing, mice were placed in the center of a custom-built Plexiglass apparatus with two open arms and two enclosed arms 1 m above floor-level. Time spent in open arms during 5 min exploration was quantified using video-tracking.

Viral-mediated tract tracing
Mice were injected with the retrograde virus AAV5-hSyn-eGFP (cat#AV-5-PV1696, University of Pennsylvania Vector Core) into BLA unilaterally (counterbalanced, from Bregma: medio-lateral +/−3.4, anterio-posterior −1.1, dorso-ventral −5.0, angle 0°) under ketamine/xylazine anesthesia to label PL→BLA neurons. Mice were allowed at least 18 days for recovery and viral expression. Post-hoc histological confirmation of BLA targeting was performed on all brains and only those meeting both viral localization and behavioral classification criteria were included.

Chemogenetic inhibition of PL→BLA pathway
An intersectional chemogenetic approach was employed to specifically target the inhibitory Designer Receptor Exclusively Activated by Designer Drugs (DREADD) hM4D(Gi) to PL→BLA neurons. AAV5-hSyn-Cre-GFP (cat#AV-5-PV1848, University of Pennsylvania Vector Core) was injected into BLA bilaterally and AAV8-hSyn-DIO-hM4D(Gi)-mCherry (cat#44362, Addgene) was injected into PL bilaterally (from Bregma: medio-lateral +/−0.8, anterio-posterior +2.3, dorso-ventral −2.3, angle 11°). Mice were allowed minimum three weeks for recovery and viral expression.

For acute PL→BLA inactivation, Clozapine-N-oxide (CNO, cat#C0832-5MG, Sigma–Aldrich, 2 mg/kg, dissolved in saline) or saline (VEH) was injected intraperitoneally (i.p.) 30 min prior to ASDS. Four mice were used to assess effect of CNO on PL and PL→BLA cFos, and for immunohisto-chemical evaluation of fidelity and efficiency of the intersectional approach. Remaining mice were allowed one week of recovery, followed by StSDS in the absence of CNO. For chronic PL→BLA inactivation, CNO (0.25 mg/ml), aspartame 0.005% or vehicle [aspartame 0.005%] was provided in drinking water ad libitum for 10 days. On day 11, mice were subjected to ASDS in absence of CNO. Post-hoc histological confirmation of injections sites was performed on all brains and only those with adequate localization of all four injection sites were categorized as DREADD-positive.

Tissue collection and processing
For tract-tracing and chemogenetic studies, mice were anesthetized with chloral hydrate (1.5 g/kg) and sacrificed by transcardial perfusion with 4% paraformaldehyde immediately after SI testing. Brains were post-fixed for 6 h and sectioned at 150 μm. Immunohistochemistry was optimized to allow visualization of entire neurons (see Extended Methods). Sections were serially stained with rabbit anti-cFos primary antibody (cat#sc-52, Santa Cruz) and Alexa Fluor-conjugated goat anti-rabbit secondary antibody (Alexa Fluor-568, cat#A-11011 for tract-tracing, or Alexa Fluor-647, cat#A-21244 for chemogenetic studies, Life Technology), followed by rabbit anti-GFP primary antibody (cat#A-11122, Life Technology) and Alexa Fluor-488-conjugated goat anti-rabbit secondary antibody (cat#A-11008, Life Technology). For all experiments, sections were incubated in 4′,6-diamidino-2-phenylindole (DAPI) for histological identification.

Imaging and image analysis
A Zeiss LSM510 confocal microscope was used for all imaging. Exact settings are included in Extended Methods. For PL→BLA cFos quantification, low resolution (10X) dual-channel 3-dimensional (3D) tile scans were acquired of medial prefrontal cortex (mPFC). For dendritic spine imaging, neighboring PL→BLA cFos immunoreactive (cFos+) and cFos non-immunoreactive (cFos−) pyramidal neurons with somas in layers II-V spanning bregma 1.9–2.2 were targeted for high resolution [100x] 3D-stacks of apical and basal dendrites.

For chemogenetic experiments, triple/quadruple-channel 3D-stacks were acquired to image GFP, mCherry, and cFos, and sometimes DAPI. For histological confirmation of injection sites, low resolution (5X) images of sections spanning entire anterio-posterior extent of PL and BLA were inspected. For CNO effects on cFos expression and the fidelity and efficiency of the intersectional chemogenetic approach, higher resolution (25X) images were acquired.

Images were imported into Fiji [39], segmented into composite channels, smoothed via mean filtering, then top-hat filtered. Object identification was performed using Foci Picker 3D [40], saved as 3D 8-bit gray-scale tiffs, and exported to MatLab for 3D-colocalization (defined as >50% overlap) using custom code. Dendritic spines were quantified semi-automatically using NeuronStudio similarly to methods previously described [41].

Statistical analyses
Statistical analyses were performed using MatLab2018b or GraphPad Prism8 and are detailed in Extended Methods. In all statistical tests, threshold was set at $p < 0.05$ and p values were adjusted to correct for multiple comparisons.

RESULTS
Development of a standardized ASDS protocol for rapid identification of susceptibility and resilience
To examine differences in PL→BLA activation during stress as a biomarker for trait vulnerability, our first objective was to develop and validate an acute stressor that identifies resilient and susceptible mice at a timepoint when the transcriptional activity marker cFos is maximally or near-maximally expressed [42–48]. In our ASDS model, male intruder C57BL/6J mice are placed into the cages of three aggressive CD1 male resident mice for two minutes each, sequentially, and tested for social avoidance one hour after onset of stress (Fig. 1). As a group, defeated mice become similarly socially avoidant following ASDS as following CSDS (Fig. S1), with no association between attack severity and SI scores (Fig. 1C). As in CSDS, mice display large individual variability in avoidant behavior following ASDS (Fig. 1D, E, Fig. S1C–D). The proportion of susceptible versus resilient mice (using conventional SI ratio ≥ 1 to define resilience) is likewise similar to CSDS, with 41 ± 5% (range 9–83%) resilience in ASDS and 45 ± 12% (range 28–93%) resilience in CSDS (Fig. 1E, Fig. S1D). Resilient and susceptible mice also show similar patterns of interaction and corner zone durations (Fig. 1F, Fig. S1E).

ASDS is not associated with pervasive depressive-like or anxiety-like behaviors but does prime for increased susceptibility to future social stress
CSDS is well-known to lead to pervasive depressive- and anxiety-like behaviors in subsets of mice [13]. Therefore, we next asked if ASDS also leads to long-term maladaptive behaviors (Fig. 2A). One week after exposure to ASDS, control and defeated mice did not differ on SI, sucrose preference, OFT, EPM, or body weight (Fig. 2B).

To assess the positive predictive value (PPV) of ASDS classification into susceptible versus resilient on chronic stress phenotyping, mice underwent ASDS then CSDS following a one-week recovery. All mice categorized as susceptible post-ASDS remained susceptible post-CSDS, meaning ASDS has a PPV of 100% for susceptibility. However, ASDS's PPV for resilience was only 18% due to a strong observed stress-priming effect. We found ASDS primes for higher susceptibility both to a subsequent CSDS (Fig. 2C, D), as well as to StSDS, a validated submaximal stressor that does not routinely induce susceptibility [49, 50] (Fig. 2E). However, while the PPV for resilience was low, resilience on initial ASDS was associated with less social avoidance after CSDS, indicating some degree of protection (Fig. S2).

Susceptible mice have a greater proportion of PL→BLA neurons activated during ASDS
To assess if differential activation of the PL→BLA pathway, a circuit involved in fear memory formation [16–18, 51, 52], is associated with divergent stress-responses to ASDS, we employed viral-mediated tract-tracing (Fig. 3A). Unilateral counterbalanced BLA
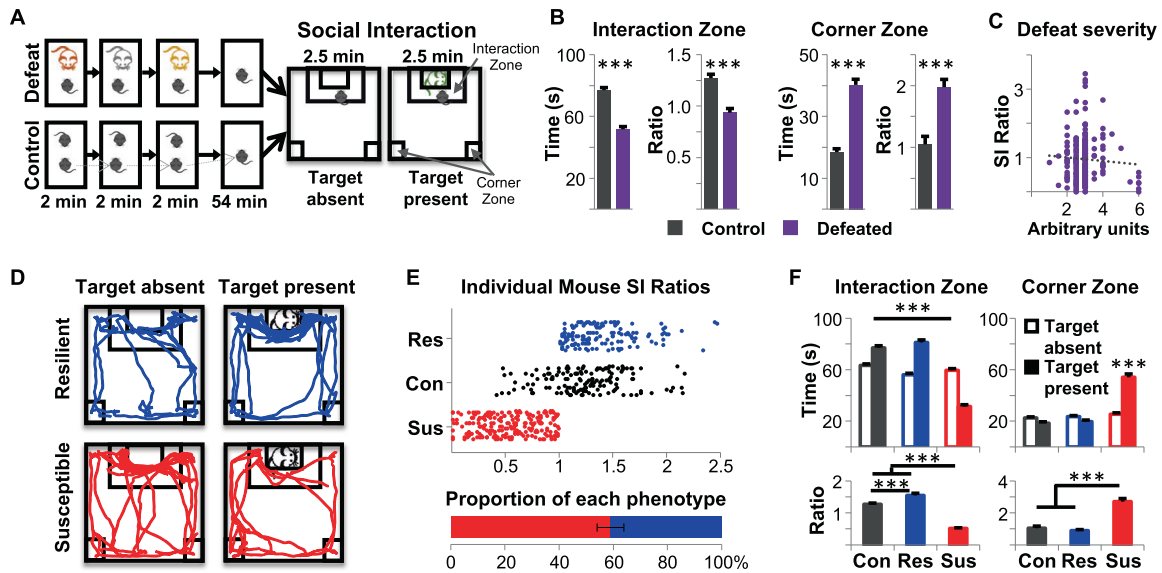
Fig. 1 Validation of a novel model of acute social defeat stress (ASDS) in male mice. A Intruder C57 mice (black mouse in figure) are placed consecutively into home cages of three novel resident mice. For defeat, resident mice are retired breeder male CD1s that screened positive for aggression. For control, resident mice are age-matched non-aggressive male C57s. The intruder C57 spends two minutes in each of the resident home cages and aggression occurs during each encounter with a CD1 but not conspecific mouse. The intruder mouse is then singly housed in a clean, empty cage for 54 min and immediately tested on social interaction (SI). For SI, the intruder C57 is first placed into an arena containing an empty enclosure and allowed to explore for 150 s. A non-aggressive CD1 "target" mouse is then placed in the enclosure and the intruder C57 is allowed to explore for another 150 s. Movement is video-recorded and the time spent in interaction zone and corner zones is quantified. **B** Defeated intruder C57 mice spend significantly less absolute and ratio of time in interaction zone, and more absolute and ratio of time in the corner zone, when target present versus absent compared to controls ($n = 149$ control, $n = 359$ defeated, two-tailed unpaired t test, SI ratio $t(506) = 5.02$, interaction time $t(506) = 8.80$, corner ratio $t(506) = 4.38$, corner time $t(506) = 7.42$, $p < 0.0001$ for all comparisons). **C** Defeat severity for each of the three individual defeat encounters of ASDS was logged in real-time during ASDS experiments for a subset of mice ($n = 256$) as follows: 0 – no attack bout occurred, 0.5 – minimal attacks (one or a few scattered and short-lived attack bouts), 1 – moderate number of attacks but not sustained throughout the two-minute period, 2 – severe and sustained attacks throughout the two-minute period. An aggregate defeat severity score was then generated by summing up the scores from an ASDS session to look for an association between attack severity and social avoidance. We found no correlation between the attack severity score and the SI scores of defeated mice ($n = 264$, r $= -0.059$, $p = 0.33$) (**D**) Susceptibility is defined as SI ratio < 1. Resilience is defined as SI ratio ≥ 1. Representative movement of a susceptible and a resilient mouse in the arena when target is absent versus present, showing the typical social approach of a resilient mouse and the social avoidance of a susceptible mouse. **E** Distribution of SI ratios of individual control (Con, black, $n = 149$), resilient (Res, blue, $n = 146$; note $n = 4$ mice with SI > 2.5 not depicted), and susceptible (Sus, red, $n = 213$) mice. Defeated mice are predominantly susceptible (59% ± 5%, $n = 17$ experiments). **F** Absolute and ratio time spent interacting with target mouse and absolute and ratio time spent in corner zones shown following classification into susceptible versus resilient. Two-way ANOVAs were performed to compare interaction and corner times and one-way ANOVAs were performed to compare ratio scores. Bonferroni post-hoc tests were performed on all ANOVAs. Control ($n = 149$) and resilient ($n = 146$) mice spent significantly more time in the interaction zone when target was present than susceptible ($n = 213$) mice [two-way ANOVA, GroupXTarget interaction $F(2, 505) = 281$ $p < 0.0001$, Group main effect: $F(2, 505) = 152$ $p < 0.0001$, Target main effect: $F(1, 505) = 12.2$ $p = 0.0005$; post-hoc tests: No target: CvR $p = 0.003$; Target: CvS $p < 0.0001$, RvS $p < 0.0001$], and had higher SI ratios [one-way ANOVA, $F(2, 505) = 182$ $p < 0.0001$, RvS $p < 0.0001$, CvS $p < 0.0001$, CvR $p < 0.0001$]. Conversely, susceptible mice spent more time in corner zones [two-way ANOVA, GroupXTarget interaction $F(2, 505) = 86$ $p < 0.0001$, Group main effect $F(2, 505) = 92$ $p < 0.0001$, Target main effect $F(1, 505) = 31$ $p < 0.0001$; post-hoc tests: Target CvS $p < 0.0001$, RvS $p < 0.0001$] and had higher corner time ratios [one-way ANOVA $F(2, 505) = 45$ $p < 0.0001$, RvS $p < 0.0001$, CvS $p < 0.0001$] compared to susceptible mice. n.s. not significant, C control, R resilient, S susceptible; *$p < 0.05$; ***$P < 0.001$.

injections of a retrograde virus were used to quantify percentage of PL→BLA neurons that are cFos+ following ASDS. Viral injections did not affect ASDS-induced behavioral responses (Fig. S3). Prefrontal sections from control, susceptible and resilient mice with histologically confirmed BLA injections (Fig. 3B) were double-stained against GFP and cFos (Fig. 3C).

Somewhat surprisingly, we found no difference in density of cFos puncta in the PL between any of the groups, suggesting physical aggression does not activate the PL differently from exposure to a novel social experience (Fig. 3D–E). There was also no difference in PL density of GFP-labeled neurons between groups (Fig. 3F). Consistent with our hypothesis, susceptible, but not resilient mice, had significantly higher proportion of GFP-labeled neurons double-stained for cFos compared to control mice (Fig. 3G). This difference was specific to PL, with no differences in proportion of activated BLA-projection neurons in neighboring anterior cingulate (AC) or infralimbic (IL) mPFC subregions (Fig. S4).

Dendritic spine differences suggest higher excitatory drive in PL→BLA neurons of susceptible mice

We next investigated differences in dendritic spines, the primary sites of excitatory synaptic inputs to cortical neurons [53–55], as a potential structural mechanism for observed higher PL→BLA activation in susceptible mice. Apical and basal dendritic segments from cFos+ and neighboring cFos− PL→BLA neurons were targeted for detailed 3D spine morphometric analyses (Fig. 3H, Fig. S5). We first investigated the impact of activation by comparing dendritic spines between cFos+ and cFos− neurons within each group, but found little evidence of systematic activity-dependent regulation of dendritic spine density or size in any spine subtype (Fig. S6). Next, we investigated the role of stress by comparisons between the stress group (resilient+susceptible) and the control group. Interestingly, spine density did not differ in any spine subtype for either cFos+ or cFos− neurons, though a stress-induced increase in spine head diameter and length was observed across most spine types and was unexpectedly more pronounced in cFos− neurons (Fig. S7).
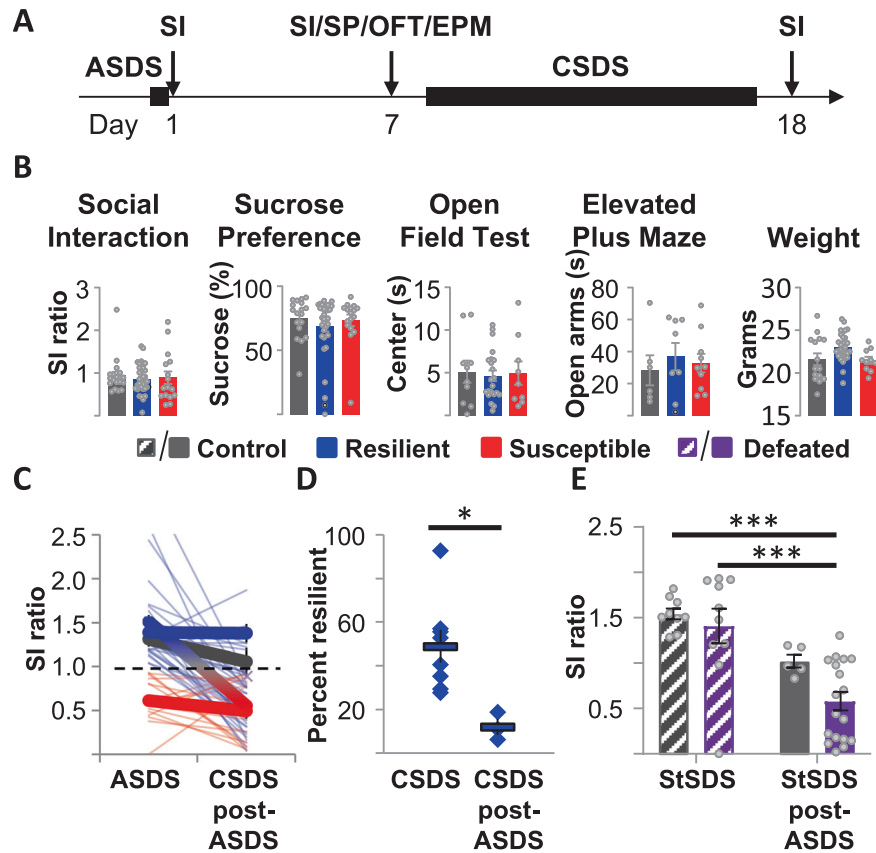
Fig. 2 **ASDS is not associated with pervasive depressive-like or anxiety-like behaviors but does prime for increased susceptibility to future social stress. A** Experimental timeline. Mice first underwent ASDS and SI testing on Day 1. One week later, weights (control $n = 24$, susceptible $n = 28$, resilient $n = 44$) were collected and different subsets of mice were tested on SI (control $n = 20$, susceptible $n = 16$, resilient $n = 34$), sucrose preference (SP, control $n = 18$, susceptible $n = 17$, resilient $n = 35$), open field test (OFT, control $n = 10$, susceptible $n = 9$, resilient $n = 22$), and/or elevated plus maze (EPM, control $n = 6$, susceptible $n = 10$, resilient $n = 8$). A subset of mice were then placed into CSDS. CSDS concluded on Day 17 and mice underwent SI on Day 18. **B** There was no significant difference between control, resilient, and susceptible mice in any of the tests performed on Day 7 [one-way ANOVA, SI $F(2, 67) = 0.24$ $p = 0.79$; SP $F(2, 67) = 0.67$ $p = 0.51$; OFT $F(2, 38) = 0.071$ $p = 0.93$; EPM $F(2, 21) = 0.27$ $p = 0.77$; Weight $F(2, 93) = 1.56$ $p = 0.22$]. **C** All mice classified as susceptible after ASDS were also classified as susceptible after CSDS (PPV = 100%). Only 18% of mice that were classified as resilient after ASDS remained resilient after CSDS, with 82% becoming susceptible (PPV = 18%). There was no significant correlation between the SI ratio post-ASDS and the SI ratio post-CSDS for any group (Pearson correlation, control: $r = -0.31$, $p = 0.17$, resilient: $r = -0.017$, $p = 0.92$, susceptible: $r = -0.15$, $p = 0.59$). There was a significant decline in the SI ratio post-CSDS as compared to the SI ratio post-ASDS for stressed (mean post-ASDS 1.21 ± 0.08, mean post-CSDS 0.63 ± 0.06, two-tailed pared T-test, $t(49) = 6.26$, $p < 0.0001$), but not control mice (mean post-ASDS 1.31 ± 0.09, mean post-CSDS 1.06 ± 0.16, two-tailed paired T-test, $t(19) = 1.276$, $p = 0.217$). **D** Percentage of CSDS-defeated mice classified as resilient when CSDS occurs post-ASDS ($12 \pm 3.6\%$) is significantly lower than when CSDS is performed on naïve mice ($49 \pm 7.5\%$, two-way unpaired T-test, $t(9) = 2.88$, $p = 0.018$). **E** Naïve mice do not show social avoidance following StSDS. In contrast, when StSDS occurs post-ASDS, defeated mice have significantly lower SI ratios (two-way ANOVA with Tukey correction, StSDSXPriming $F(1, 38) = 1.137$ $p = 0.293$, StSDS $F(1, 38) = 3.943$ $p = 0.0543$, Priming $F(1, 38) = 21.78$ $p < 0.0001$, primed StSDS defeated v naïve StSDS defeated $p < 0.0001$, primed StSDS defeated v naïve StSDS controls $p < 0.0001$). *$p < 0.05$, ***$p < 0.001$.

Despite no stress-associated differences in spine density, susceptible mice had significantly higher mushroom spine density than resilient mice, specifically on basal dendrites of cFos+ PL→BLA neurons (Fig. 3I, Fig. S8A). No differences were found in the spine densities of cFos− neurons. Resilient and susceptible mice had larger thin spine head diameters and lengths than controls across cFos+ and cFos− neurons (Fig. 3J, K, Fig. S8B, C), but the magnitude was higher in susceptible mice in several instances. In addition, susceptible mice had significantly larger mushroom spine size than resilient mice, though neither group differed significantly from control.

In summary, we identified complex and unique PL→BLA dendritic spine morphological signatures in susceptible versus resilient mice that cannot be explained by activity-dependent regulation (Fig. 4). They are also unlikely to be solely due to stress-induced plasticity given that most differences identified specifically in susceptible versus resilient comparisons are related to

mushroom spines, which are generally considered to be the most stable subtype [53, 56, 57]. Thus, a higher number and larger size of PL→BLA mushroom spines might represent the structural substrate for aberrant overactivation of this pathway in susceptible mice.

Chemogenetic inhibition of the PL→BLA pathway during or prior to ASDS blocks stress-induced social avoidance

To test the hypothesis that PL→BLA overactivation during ASDS mediates the susceptible behavioral response, we used an intersectional chemogenetic approach to deliver an inhibitory DREADD to this pathway (Fig. 5A–C, Fig. S9). In our first experiment, CNO was administered systemically only once, 30 min prior to ASDS. CNO treatment in animals with histologically confirmed injections was found to decrease cFos both overall in the PL, as well as specifically in PL→BLA neurons (Fig. 5D–F). Consistent with our hypothesis, VEH-injected defeated mice
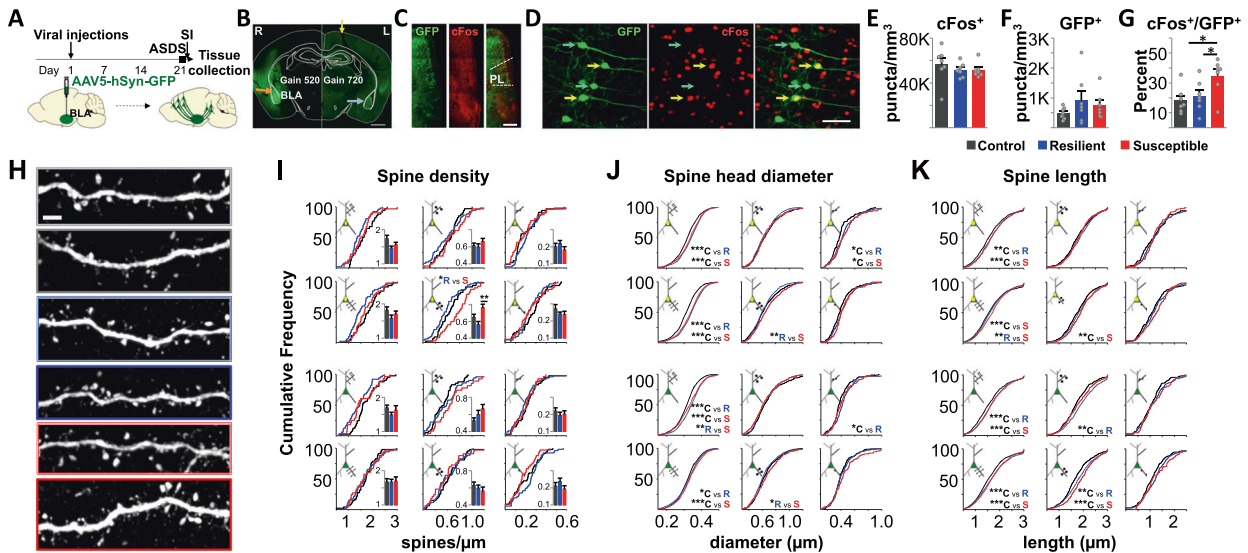
Fig. 3 Susceptible mice exhibit structure/function differences in prelimbic to basolateral amygdala (PL→BLA) neurons suggestive of overactivation of this circuit during ASDS. A Schematic of experimental design and timeline. A retrograde GFP-expressing virus was injected unilaterally in the BLA on Day 1. Twenty-one days later, mice underwent ASDS and SI, followed by immediate sacrifice and tissue collection. **B** Representative image of BLA injection. Outline overlay was taken from The Mouse Brain, 2nd Ed by George Paxinos and Keith Franklin (scale bar 1 mm, plate 42, Bregma −1.34). Hemispheres were marked with a "nick" in the left hemisphere (yellow arrow, showing cut in retrosplenial cortex). Post-hoc histological confirmation of injection site was performed on all brains and inclusion criteria were defined as dense expression of GFP in injected BLA (orange arrow, hemisphere imaged at a lower gain of 520) and in contralateral BLA (blue arrow, hemisphere imaged at higher gain of 720 to show BLA→BLA projecting neurons). **C** Representative image (scale bar 0.5 mm) of anti-GFP and anti-cFos stained medial prefrontal cortex (mPFC) with demarcated PL (Paxinos atlas, plate 14, bregma 1.98). **D** Representative higher resolution image (scale bar 200 µm) of anti-GFP and anti-cFos staining in PL. Images were analyzed in 3D and PL→BLA neurons (as evidenced by anti-GFP staining) were classified as cFos positive (cFos+, yellow arrows) or cFos negative (cFos−, green arrows). **E** No significant difference in number of PL cFos puncta was observed between control, resilient, and susceptible mice [$n = 7$ control mice, $n = 7$ resilient mice, $n = 7$ susceptible mice; $n = 1539–6628$ cells/animal ($n = 30,495$ total cells) control, $n = 2942–4654$ cells/animal ($n = 26,505$ total cells) resilient, $n = 3183–5504$ cells/animal ($n = 31,906$ total cells) susceptible, one-way ANOVA $F(2, 18) = 1.1$, $p = 0.36$]. **F** No significant difference in number of GFP neurons was observed between control, resilient, and susceptible mice [$n = 7$ control mice, $n = 7$ resilient mice, $n = 7$ susceptible mice; $n = 14–63$ cells/ animal ($n = 257$ total cells) control, $n = 16–170$ cells/animal ($n = 404$ total cells) resilient, $n = 28–110$ cells/animal ($n = 445$ total cells) susceptible, one-way ANOVA $F(2, 18) = 0.54$ $p = 0.59$]. **G** Susceptible mice had significantly higher proportion cFos+ GFP-expressing neurons than resilient and control mice [$n = 7$ control mice, $n = 7$ resilient mice, $n = 7$ susceptible mice; $n = 2–22$ cells/animal ($n = 55$ total cells) control, $n = 1–31$ cells/animal ($n = 85$ total cells) resilient, $n = 11–32$ cells/animal ($n = 136$ total cells) susceptible, one-way ANOVA $F(2, 18) = 5.0$ $p = 0.019$, post-hoc Bonferroni test: C vs S 0.012, R vs S 0.042, C vs R 0.56]. **H** Representative images of apical and basal dendrites from cFos+ neurons (scale bar 3 µm; gray outline from control; blue outline from resilient; red outline from susceptible). Single width outlines indicate basal dendrites and double width outlines indicate apical dendrites. Imaged and analyzed dataset consisted of: 78 dendrites from 21 cFos+ neurons and 88 dendrites from 21 cFos− neurons from control mice, 105 dendrites from 28 cFos+ neurons and 102 dendrites from 28 cFos− neurons from resilient mice, and 69 dendrites from 18 cFos+ neurons and 60 dendrites from 18 cFos– neurons from susceptible mice. **I** Spine subtypes are separated by column and indicated by the cartoon at the top. cFos+ and cFos− neurons are indicated in the cartoon by yellow oval or no oval, respectively, in the green soma. Spine subtype is shown by length and size of protuberances in cartoon. Thin spines are long and small (left column), mushroom spines are large and long (middle column), and stubby spines are short (right column). Black represents data from controls, blue from resilient, and red from susceptible. For all distributions, the reported p value represents K-S test with Bonferroni correction at the level of the individual test. CDF plots and group averages (insets) of density of spine subtypes on apical and basal dendrites of cFos+ and cFos− neurons. The only identified significant difference was in the mushroom spines on basal dendrites of cFos+ neurons, where susceptible mice had a higher density than resilient mice both when analyzed by group average (one-way ANOVA, $F(2, 62)$ $p = 0.004$, Bonferroni post-hoc, RvsS $p = 0.0057$) and by distribution of densities ($p = 0.023$). **J** CDF plots of spine head diameters. Resilient and susceptible mice had significantly larger thin spine heads than controls on all dendritic compartments across both cFos+ and cFos− neurons (thin cFos+ apical CvsR $p < 0.0001$; thin cFos+ apical CvsS $p < 0.0001$; thin cFos+ basal CvsR $p < 0.0001$; thin cFos+ basal CvsS $p < 0.0001$; thin cFos− apical CvsR $p < 0.0001$; thin cFos− apical CvsS $p < 0.0001$; thin cFos− basal CvsR $p = 0.0363$; thin cFos− basal CvsR $p = 0.0006$). Thin spines on the apical dendrites of cFos− neurons of resilient mice were larger than their counterparts on neurons from susceptible mice (thin cFos− apical RvsS $p = 0.0074$). Mushroom spine size did not differ between control and either susceptible or resilient mice, but did differ between the two stress groups, with susceptible mice having significantly larger mushroom spines than resilient on the basal dendrites of both cFos+ and cFos− neurons (mushroom cFos+ basal SvsR $p = 0.0036$; mushroom cFos− basal SvsR $p = 0.013$). Stubby spines were larger than controls in for both susceptible and resilient mice in certain dendritic compartments (stubby cFos+ apical CvsR $p = 0.009$; stubby cFos+ apical CvsS $p = 0.039$; stubby cFos+ apical CvsR $p = 0.0045$). **K** CDF plots of spine lengths. Similar to spine head size, thin spine length was indiscriminately higher than control for both resilient and susceptible mice in most dendritic compartments (thin cFos+ apical CvsR $p = 0.0044$, thin cFos+ apical CvsS $p = 0.0009$; thin cFos+ basal CvsS $p < 0.0001$; thin cFos− apical/basal CvsR $p = 0.0002$, apical/basal CvsS $p < 0.0001$; thin cFos− apical/basal CvsR $p = 0.0002$, apical/basal CvsS $p < 0.0001$). Susceptible mice had significantly longer thin spines than resilient mice in one dendritic compartment (thin cFos+ basal SvsR $p = 0.0094$). Mushroom spines were longer than controls for both susceptible and resilient mice in several dendritic compartments, mostly on cFos− neurons (mushroom cFos+ basal CvsS $p = 0.0064$; mushroom cFos− apical CvsR $p = 0.0002$; mushroom cFos− basal CvsR $p = 0.0002$; mushroom cFos− basal CvsS $p < 0.0001$). No differences in the length of stubby spines were observed in any dendritic compartment between any group. C control, R resilient, S susceptible; *$p < 0.05$; **$P < 0.01$; ***$P < 0.001$.

Fig. 4 Summary of PL→BLA structure/function differences in resilient versus susceptible mice.

FUNCTION		STRUCTURE								
Neuron Activation	Dendrite	Spine density Thin	Spine density Mushroom	Spine density Stubby	Spine head diameter Thin	Spine head diameter Mushroom	Spine head diameter Stubby	Spine length Thin	Spine length Mushroom	Spine length Stubby
red↑ / blue↓ (cFos+ Apical)	Apical	n.s.	n.s.	n.s.	↑(R) ↑(B)	n.s.	↑(R) ↑(B)	↑(R) ↑(B)	n.s.	n.s
(cFos+ Basal)	Basal	n.s.	↓(B)	n.s.	↑(R) ↑(B)	↓(B)	n.s.	↑↓(R) ↑(B)	↑(R)	n.s
(cFos− Apical)	Apical	n.s.	n.s.	n.s.	↑↓(R) ↑(B)	n.s.	↑(B)	↑(R) ↑(B)	↑(B)	n.s
(cFos− Basal)	Basal	n.s.	n.s.	n.s.	↑(R) ↑(B)	↓(B)	n.s.	↑(R) ↑(B)	↑(R) ↑(B)	n.s.

Unidirectional arrows indicate the structure/function index for the group associated with that color (red represents susceptible, blue represents resilient) is significantly greater than controls. Bidirectional arrows represent comparisons between susceptible and resilient mice. The structure/function index for the group represented by the color in upper half of the arrow was found to be significantly greater than the group represented in the lower half of the arrow. n.s. indicates that no significant difference was identified between any of the groups. Susceptible mice had a larger proportion of PL→BLA neurons activated compared to controls and resilient. Thin spines from both susceptible and resilient mice were larger than control in both head diameter and length, and this difference was indiscriminate to cFos-status. To a lesser extent, stubby spines also were found to be larger in the two stress groups than in controls. Mushroom spines, however, showed a unique pattern with differences in both density and spine head diameter restricted to susceptible versus resilient comparisons, with no stress-associated difference in these indices. Altogether, these findings suggest global stress-induced regulation of thin spines and preexisting differences in mushroom spines acting as a potential substrate for overexcitability of this pathway during ASDS.

showed a typical pattern of social avoidance, while CNO-injected defeated mice did not differ from controls in their interaction with a novel mouse or time spent in corner zones (Fig. 5G). To test if the effects of inhibiting the PL→BLA extended to blocking ASDS-induced priming to increased susceptibility to future social stress, mice were also tested on StSDS in the absence of CNO following a one-week recovery (Fig. 5H). As expected, mice that received VEH during ASDS showed a priming effect, displaying social avoidance following StSDS. In contrast, the priming effect was blocked in previously defeated mice that had been CNO-treated during ASDS, also implicating the PL→BLA in ASDS fear memory acquisition, rather than solely in fear expression.

In our second experiment, we asked if long-term inhibition of the PL→BLA would remain effective in blocking ASDS-induced social avoidance. CNO or vehicle was added to the drinking water and provided ad libitum for 10 days (Fig. 5I). On day 11, mice underwent ASDS without CNO administration. Similar to acute CNO administration, chronically CNO-treated defeated mice showed control level social interaction while vehicle treated mice showed the typical pattern of social avoidance. For both experiments, animals excluded on the basis of lacking DREADD expression on post-hoc histological investigation showed ASDS-induced social avoidance in both VEH- and CNO-treated groups (Fig. S10) despite observed off-target anxiolytic effects of chronic CNO on OFT (Fig. S11).

DISCUSSION
We present data on a novel acute stressor that uniquely, rapidly, and reproducibly classifies male mice into stress-susceptible versus stress-resilient. ASDS mirrors CSDS population distribution of social avoidance one-hour post-stress, does not induce CSDS-phenotypic long-term maladaptive behaviors, but primes for increased social avoidance following future social stress. While changes in behavior upon retesting SI in mice following CSDS have previously been observed [58], the strong priming effect observed here, with a majority of resilient mice becoming susceptible, suggests memory acquisition occurs despite no changes in baseline behavior. Although the comparison between ASDS and CSDS is limited by the ASDS-induced priming effect, these models likely tap into overlapping behavioral endophenotypes. This is supported by (i) the striking consistency in distributions of susceptibility and resilience on ASDS versus CSDS; (ii) all mice that remain resilient post-CSDS were originally classified as resilient post-ASDS, and (iii) resilience on ASDS

confers some protection from subsequent CSDS-induced social avoidance.

Our novel stress paradigm was developed to offer a window into the contribution of the initial stress-activated neurocircuits to individual variability in stress-responses. We identified several structure/function differences in ASDS-activated PL→BLA neurons, a pathway highly implicated in fear acquisition and expression across multiple stressors [16–18, 52, 59–63]. First, we found a higher proportion of PL→BLA neuron transcriptional activation in susceptible mice. Second, we found a higher density and size of mushroom spines in transcriptionally activated PL→BLA neurons in susceptible mice. These findings implicate PL→BLA over-activation during a first-time stressor as a biomarker of trait vulnerability, though we note this might be context-dependent to social stress [64]. In accordance with this hypothesis, and consistent with the literature implicating this circuit in fear expression [18, 22, 62, 63, 65–67], we found inhibiting this pathway during ASDS blocked stress-induced social avoidance selectively in DREADD expressing mice.

Importantly, inactivation of PL→BLA during ASDS also blocked ASDS-induced priming to future stress. CNO-dependent blocking of stress-priming occurred one-week post-CNO administration, indicating that observed effects are attributable to PL→BLA inactivation during ASDS rather than off-target drug effects. Consistent with this pathway's additional role in fear memory consolidation [21, 65, 68–72], our data suggest that blocking the PL→BLA pathway does not merely block stress-induced fear expression, but also fear memory acquisition and/or consolidation. However, an important caveat of the intersectional chemogenetic manipulation used here is potential unintended additional inhibition of axonal collaterals of the targeted PL→BLA neurons, which were not assessed. Therefore, our results might be most representative of the function of BLA-projecting PL neurons rather than the PL→BLA pathway.

Identified morphological differences between susceptible and resilient mice are intriguing and could reflect either preexisting differences in spine subtype densities, or differences in spine plasticity. Interestingly, differences in mushroom spines were restricted to susceptible versus resilient comparisons, with no differences observed between control versus resilient, control versus susceptible, or between control and the combined (resilient + susceptible) stress group. Using slice physiology and a different stress model, Wang et al. showed rapid and opposing changes in excitatory transmission in cFos+ PL neurons from susceptible versus resilient mice [73]. Our mushroom spine

Figure A–I
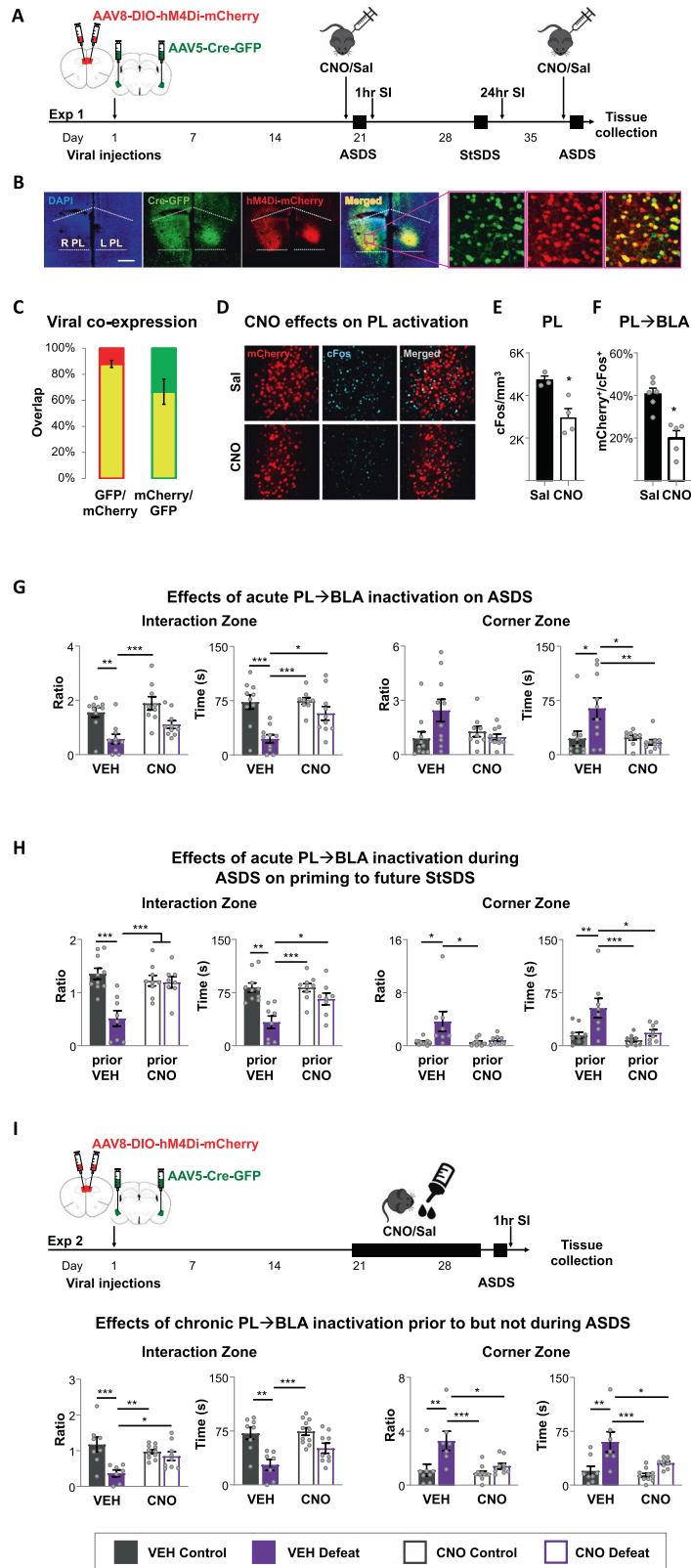
differences could reflect the morphological mechanisms for this type of rapid plasticity. Mushroom spines are known for their stability [53, 56, 57, 74–77], but changes in spine size have been reported on the order of minutes to hours [55–57, 78–80]. However, in vivo observations of dendritic spine formation indicate that large spines form by enlarging preexisting smaller spines [53, 81]. Therefore, rapid stress-induced maturation of thin spines into mushroom spines in susceptible mice is unlikely sans compensatory decrease in thin or stubby spine density. In contrast, thin spine head diameter and length showed an

Fig. 5 Chemogenetic inhibition of PL→BLA during and prior to ASDS blocks stress-induced social avoidance and priming to increased susceptibility to future social stress. A Experimental timeline for acute chemogenetic inhibition. Mice were stereotactically injected with a retrograde Cre-GFP-carrying virus in BLA bilaterally and a Cre-dependent hM4D(Gi)-mCherry-carrying virus in PL bilaterally. Following three weeks recovery, mice were injected intraperitoneally (i.p.) with either saline (VEH) or CNO dissolved in saline 30 min prior to ASDS. One week later, a small subset of mice underwent another ASDS and SI in the presence of CNO or VEH, in order to collect brains for studies looking at CNO effects on cFos and the fidelity and efficiency of the intersectional chemogenetic approach. Remaining mice were subjected to StSDS on day 28 and were tested on SI 24 h later. All mice were then sacrificed and brains collected for histological examination of viral injections. **B** Representative PL image (scale bar 0.5 mm) of intersectional viral approach. Inset (pink outline) shows a portion of the PL at higher resolution (scale bar 200 µm). Colocalized hM4D(Gi)-mCherry/Cre-GFP appear yellow in merged image on right. **C** Intersectional approach showed high fidelity [89%±5 of hM4D(Gi) puncta (red) colocalized with Cre puncta (green)] and moderately high efficiency [68%±20% of Cre puncta colocalized with hM4D(Gi) puncta]. **D** Representative image (scale bar 200 µm) of hM4D(Gi)-mCherry (red) and cFos (cyan) after i.p. VEH or CNO 30 min prior to ASDS and SI, followed by immediate sacrifice. **E** Significantly lower cFos density (two-tailed unpaired T-test, $t(4) = 3.88$, $p = 0.018$) was observed in the PL of CNO- compared to VEH-injected mice. **F** Significantly fewer cells expressing hM4D(Gi) (red) co-expressed cFos (cyan) in CNO- compared to VEH-injected mice (two-tailed unpaired T-test, $t(8) = 4.692$, $p = 0.0015$). **G–I** For all group comparisons, two-way ANOVA with post-hoc Tukey correction were used to test drug by stress interactions (DrugXStress), main stress effects (stress), main drug effects (drug), and individual differences between control (C, dark gray) and defeated (D, purple) mice treated with VEH (filled bars) versus CNO (empty bars). Comparisons were done for hM4D(Gi)+ mice, defined as histologically verified targeting of all four injection sites. **G** Effects of PL→BLA inhibition during ASDS. SI ratio, corner ratio, and absolute time in the interaction zone and corner zones was compared between hM4D(Gi)+ mice in VEH (control $n = 10$, defeat $n = 10$) versus CNO groups (control $n = 9$, defeat $n = 10$). In contrast to VEH-injected mice, which showed a typical pattern of social avoidance following ASDS, CNO injected defeated mice had control-level SI ratios [DrugXStress $F(1, 35) = 0.45$, $p = 0.60$, stress $F(1, 35) = 36$ $p < 0.0001$, drug $F(1, 35) = 8.6$ $p = 0.026$, VEH C v VEH D $p = 0.0034$, VEH D v CNO C $p = 0.0001$], interaction times [DrugXStress $F(1, 35) = 7.1$, $p = 0.040$, stress $F(1, 35) = 29$ $p < 0.0001$, drug $F(1, 35) = 8.5$ $p = 0.025$, VEH C v VEH D $p = 0.0003$, CNO C v VEH D $p = 0.0003$, VEH D v CNO D $p = 0.017$], time in corner zone [DrugXStress $F(1, 35) = 13$, $p = 0.015$, stress $F(1, 35) = 6.6$ $p = 0.074$, drug $F(1, 35) = 11$ $p = 0.022$, VEH C v VEH D $p = 0.02$, CNO C v VEH D $p = 0.033$, VEH D v CNO D $p = 0.0066$, and corner ratios [DrugXStress $F(1, 35) = 12$, $p = 0.026$, stress $F(1, 35) = 5.4$ $p = 0.13$, drug $F(1, 35) = 4.1$ $p = 0.18$], with three of these four indices showing significant DrugXStress interaction. **H** Effects of PL→BLA inhibition during ASDS on priming to susceptibility on subsequent StSDS. VEH (control $n = 10$, defeat $n = 8$) versus CNO (control $n = 9$, defeat $n = 8$) refers to administration during ASDS. No drug was administered during StSDS. The Grubb's outlier test identified an outlier mouse for corner ratio ($G(8) = 2.34$, $p = 0.003$) and therefore this mouse was removed from the significance testing for this index; however, because the remainder of the behavioral indices for this mouse did not reach criteria for outlier [interaction zone ($G(8) = 1.14$, $p = 0.25$), SI ratio ($G(8) = 1.08$, $p = 0.28$), and absolute time in the corners ($G(8) = 2.08$, $p = 0.07$)], the mouse was included in the rest of the significance testing and also was included in all four subfigures. CNO administration during ASDS protected hM4D(Gi)+ mice from stress-priming effects as evidenced by control-level SI ratios [DrugXStress $F(1, 31) = 20$, $p = 0.0013$, stress $F(1, 31) = 23$ $p = 0.0006$, drug $F(1, 31) = 9.2$ $p = 0.022$, VEH C v VEH D $p < 0.0001$, CNO C v VEH D $p = 0.0009$, VEH D v CNO D $p = 0.002$], interaction times [DrugXStress $F(1, 31) = 8.5$, $p = 0.03$, stress $F(1, 31) = 33$ $p < 0.0001$, drug $F(1, 31) = 8.3$ $p = 0.032$, VEH C v VEH D $p = 0.002$, CNO C v VEH D $p = 0.0003$, VEH D v CNO D $p = 0.027$], corner times [DrugXStress $F(1, 31) = 7.1$, $p = 0.059$, stress $F(1, 31) = 22$ $p = 0.0017$, drug $F(1, 31) = 16$ $p = 0.0061$, VEH C v VEH D $p = 0.0032$, CNO C v VEH D $p = 0.0006$, VEH D v CNO D $p = 0.0134$], and corner ratios [DrugXStress $F(1, 30) = 5.6$, $p = 0.025$, stress $F(1, 30) = 12.3$ $p = 0.001$, drug $F(1, 30) = 6$ $p = 0.02$, VEH C v VEH D $p = 0.002$, CNO C v VEH D $p = 0.002$, CNO D v VEH D $p = 0.02$], with significant DrugXStress interactions in three of the four indices and trend toward significance in the fourth index. **I** Experimental timeline for chronic chemogenetic inhibition of PL→BLA. Same intersectional chemogenetic approach and *post-hoc* histological inspection of injection sites was performed as described above. Following three-week recovery, mice were given either CNO or vehicle-treated (aspartame) drinking water ad libitum for 10 days. On Day 11, regular drinking water was provided in the morning and mice underwent ASDS and SI in the afternoon. As in the case of acute CNO administration, VEH-treated (control $n = 8$, defeat $n = 7$) hM4D(Gi)+ mice showed the typical pattern of social avoidance following ASDS, but CNO-treated mice (control $n = 11$, defeat $n = 9$) showed partial protection from the phenotypic decreased SI ratios [DrugXStress $F(1, 31) = 7.4$, $p = 0.011$, stress $F(1, 31) = 14$ $p = 0.0008$, drug $F(1, 31) = 1.2$ $p = 0.28$, VEH C v VEH D $p = 0.0010$, VEH D v CNO D $p = 0.028$, VEH D v CNO C $p = 0.0095$], interaction times [DrugXStress $F(1, 31) = 2.2$, $p = 0.15$, stress $F(1, 31) = 17$ $p < 0.0001$, drug $F(1, 31) = 3.4$ $p = 0.073$, VEH C v VEH D $p = 0.0012$, VEH D v CNO C $p = 0.0002$, VEH D v CNO D $p = 0.070$], increased corner zone time [DrugXStress $F(1, 31) = 3.1$, $p = 0.090$, stress $F(1, 31) = 18$ $p = 0.0002$, drug $F(1, 31) = 7.0$ $p = 0.013$, VEH C v VEH D $p = 0.002$, VEH D v CNO C $p = 0.0002$, VEH D v CNO D $p = 0.027$], and corner ratio [DrugXStress $F(1, 31) = 4.7$, $p = 0.039$, stress $F(1, 31) = 13$ $p = 0.0013$, drug $F(1, 31) = 7.6$ $p = 0.0097$, VEH C v VEH D $p = 0.0036$, VEH D v CNO C $p = 0.0005$, VEH D v CNO D $p = 0.011$]. Two of these indices (SI ratio and corner ratio) reached significant DrugxStress interactions. C control, R resilient, S susceptible, *$p < 0.05$; **$P < 0.01$; ***$P < 0.001$.

indiscriminate and equal magnitude stress-induced increase in both resilient and susceptible mice across cFos+ and cFos− neurons. Thin spines are well-documented to be more plastic than mushroom spines [53, 56, 57, 76–78, 82–91] and consistent with our stress-induced findings, prior work has shown that thin spines rapidly change in response to systemic stress hormones [23, 57, 92, 93]. Taken together, our observed thin spine differences serve as a positive control of stress-induced plasticity, whereas identified mushroom spine density and size differences are specifically associated with individual variability in stress-response.

Interestingly, stress-induced effects on PL neurons have mostly been observed in apical dendrites [84, 94–96], while our mushroom spine density difference was exclusive to basal dendrites. The source of input to the more numerous and larger mushroom spines on PL→BLA neurons from susceptible mice remains uncertain. There is some evidence the amygdala may preferentially synapse onto basal dendrites of PL neurons [97] and activation of the reciprocal BLA→PL circuit reduces social interaction [51]. Thus, an intriguing possibility for observed

structure/function differences could be an aberrant positive feedback loop between the PL and BLA.

Given our goal of investigating potential targets for prevention, it is important to ascertain if chronic manipulations of this circuit lead to habituation and/or compensatory mechanisms that might diminish long-term benefit. We therefore also tested the effects of chronic PL→BLA inhibition by CNO administration in drinking water during the 10 days prior to ASDS. Our results show no evidence of circuit habituation or compensatory mechanisms, with chronic CNO treatment similarly effective in blocking ASDS-induced social avoidance. Furthermore, while we did observe mild CNO-induced anxiolytic effects consistent with previously reported off-target CNO drug-effects [38, 98–103], these off-target effects did not contribute to reducing ASDS-induced social avoidance given that DREADD-negative mice receiving chronic CNO showed the expected pattern of post-ASDS social avoidance. Together, these data show CNO did not have off-target effects on the behavior of interest.

The results presented here indicate that modulation of the PL→BLA circuit prior to and/or during stress might be an effective

target for promoting stress-resilience in male mice. While novel models of female social defeat are emerging [104–106], these remain limited and circuit responses in female mice have been minimally explored. Therefore, for feasibility, here we restricted our scope to the development of an acute model that parallels the well-validated CSDS model in male mice. It should be noted that excessive activation of the prefrontal to amygdala pathway has been reported in humans with early life adversity and adult neuropsychiatric disorders, including in females [107–116]. Therefore, an important next step will be to develop a parallel social stress model in female mice and probe the contribution of the PL→BLA circuit to susceptibility. Additional next steps include ascertaining if chronic manipulations can "rewire" the PL→BLA circuit to induce a lasting resilient state, identifying the structural changes associated with rewiring, and assessing the duration of preventative protection against stress.

REFERENCES

1. Reddy MS. Depression: the disorder and the burden. Indian J Psychol Med. 2010;32:1–2.
2. Lehmann ML, Herkenham M. Environmental enrichment confers stress resiliency to social defeat through an infralimbic cortex-dependent neuroanatomical pathway. J Neurosci. 2011;31:6159–73.
3. Schloesser RJ, Lehmann M, Martinowich K, Manji HK, Herkenham M. Environmental enrichment requires adult neurogenesis to facilitate the recovery from psychosocial stress. Mol Psychiatry. 2010;15:1152–63.
4. Clinton SM, Watson SJ, Akil H. High novelty-seeking rats are resilient to negative physiological effects of the early life stress. Stress.2014;17:97–107.
5. Herringa RJ, Burghy CA, Stodola DE, Fox ME, Davidson RJ, Essex MJ. Enhanced prefrontal-amygdala connectivity following childhood adversity as a protective mechanism against internalizing in adolescence. Biol Psychiatry Cogn Neurosci Neuroimaging. 2016;1:326–34.
6. Indovina I, Robbins TW, Nunez-Elizalde AO, Dunn BD, Bishop SJ. Fear-conditioning mechanisms associated with trait vulnerability to anxiety in humans. Neuron.2011;69:563–71.
7. McCreary JK, Truica LS, Friesen B, Yao Y, Olson DM, Kovalchuk I, et al. Altered brain morphology and functional connectivity reflect a vulnerable affective state after cumulative multigenerational stress in rats. Neuroscience.2016;330:79–89.
8. Schmidt MV, Trumbach D, Weber P, Wagner K, Scharf SH, Liebl C, et al. Individual stress vulnerability is predicted by short-term memory and AMPA receptor subunit ratio in the hippocampus. J Neurosci. 2010;30:16949–58.
9. Schmidt MV, Wang XD, Meijer OC. Early life stress paradigms in rodents: potential animal models of depression? Psychopharmacol (Berl). 2011;214:131–40.
10. Morrison AP, French P, Stewart SL, Birchwood M, Fowler D, Gumley AI, et al. Early detection and intervention evaluation for people at risk of psychosis: multisite randomised controlled trial. BMJ.2012;344:e2233.
11. Bechdolf A, Wagner M, Ruhrmann S, Harrigan S, Putzfeld V, Pukrop R, et al. Preventing progression to first-episode psychosis in early initial prodromal states. Br J Psychiatry. 2012;200:22–9.
12. Lee H, Dvorak D, Kao HY, Duffy Á, Scharfman HE, Fenton AA. Early cognitive experience prevents adult deficits in a neurodevelopmental schizophrenia model. Neuron.2012;75:714–24.
13. Krishnan V, Han MH, Graham DL, Berton O, Renthal W, Russo SJ, et al. Molecular adaptations underlying susceptibility and resistance to social defeat in brain reward regions. Cell.2007;131:391–404.
14. Golden SA, Covington HE 3rd, Berton O, Russo SJ. A standardized protocol for repeated social defeat stress in mice. Nat Protoc. 2011;6:1183–91.
15. Christoffel DJ, Golden SA, Russo SJ. Structural and synaptic plasticity in stress-related disorders. Rev Neurosci. 2011;22:535–49.
16. Arruda-Carvalho M, Clem RL. Pathway-selective adjustment of prefrontal-amygdala transmission during fear encoding. J Neurosci. 2014;34:15601–9.
17. Sierra-Mercado D, Padilla-Coreano N, Quirk GJ. Dissociable roles of prelimbic and infralimbic cortices, ventral hippocampus, and basolateral amygdala in the expression and extinction of conditioned fear. Neuropsychopharmacology.2011;36:529–38.
18. Knapska E, Macias M, Mikosz M, Nowak A, Owczarek D, Wawrzyniak M, et al. Functional anatomy of neural circuits regulating fear and extinction. Proc Natl Acad Sci USA. 2012;109:17093–8.
19. McGinnis MM, Parrish BC, Chappell AM, Alexander NJ, McCool BA. Chronic Ethanol Differentially Modulates Glutamate Release from Dorsal and Ventral Prefrontal Cortical Inputs onto Rat Basolateral Amygdala Principal Neurons. eNeuro. 2020;7:1–17.
20. Tripathi SJ, Chakraborty S, Srikumar BN, Raju TR, Shankaranarayana Rao BS. Basolateral amygdalar inactivation blocks chronic stress-induced lamina-specific reduction in prefrontal cortex volume and associated anxiety-like behavior. Prog Neuropsychopharmacol Biol Psychiatry. 2019;88:194–207.
21. Arruda-Carvalho M, Clem RL. Prefrontal-amygdala fear networks come into focus. Front Syst Neurosci. 2015;9:145.
22. Pendyam S, Bravo-Rivera C, Burgos-Robles A, Sotres-Bayon F, Quirk GJ, Nair SS. Fear signaling in the prelimbic-amygdala circuit: a computational modeling and recording study. J Neurophysiol. 2013;110:844–61.
23. Carlson PJ, Singh JB, Zarate CA Jr., Drevets WC, Manji HK. Neural circuitry and neuroplasticity in mood disorders: insights for novel therapeutic targets. NeuroRx.2006;3:22–41.
24. Drevets WC, Price JL, Furey ML. Brain structural and functional abnormalities in mood disorders: implications for neurocircuitry models of depression. Brain Struct Funct. 2008;213:93–118.
25. Lee H, Heller AS, van Reekum CM, Nelson B, Davidson RJ. Amygdala-prefrontal coupling underlies individual differences in emotion regulation. Neuroimage.2012;62:1575–81.
26. Price JL, Drevets WC. Neurocircuitry of mood disorders. Neuropsychopharmacology.2010;35:192–216.
27. Siegle GJ, Thompson W, Carter CS, Steinhauer SR, Thase ME. Increased amygdala and decreased dorsolateral prefrontal BOLD responses in unipolar depression: related and independent features. Biol Psychiatry. 2007;61:198–209.
28. Urry HL, van Reekum CM, Johnstone T, Kalin NH, Thurow ME, Schaefer HS, et al. Amygdala and ventromedial prefrontal cortex are inversely coupled during regulation of negative affect and predict the diurnal pattern of cortisol secretion among older adults. J Neurosci. 2006;26:4415–25.
29. Qu Y, Yang C, Ren Q, Ma M, Dong C, Hashimoto K. Regional differences in dendritic spine density confer resilience to chronic social defeat stress. Acta Neuropsychiatr. 2018;30:117–22.
30. Zhang J, Qu Y, Chang L, Pu Y, Hashimoto K. (R)-Ketamine rapidly ameliorates the decreased spine density in the medial prefrontal cortex and hippocampus of susceptible mice after chronic social defeat stress. Int J Neuropsychopharmacol. 2019;22:675–9.
31. Colyn L, Venzala E, Marco S, Perez-Otano I, Tordera RM. Chronic social defeat stress induces sustained synaptic structural changes in the prefrontal cortex and amygdala. Behav Brain Res. 2019;373:112079.
32. Dragunow M, Faull R. The use of c-fos as a metabolic marker in neuronal pathway tracing. J Neurosci Methods. 1989;29:261–5.
33. Martinez M, Calvo-Torrent A, Herbert J. Mapping brain response to social stress in rodents with c-fos expression: a review. Stress.2002;5:3–13.
34. LaPlant Q, Vialou V, Covington HE 3rd, Dumitriu D, Feng J, Warren BL, et al. Dnmt3a regulates emotional behavior and spine plasticity in the nucleus accumbens. Nat Neurosci. 2010;13:1137–43.
35. McCann KE, Sinkiewicz DM, Rosenhauer AM, Beach LQ, Huhman KL. Transcriptomic analysis reveals sex-dependent expression patterns in the basolateral amygdala of dominant and subordinate animals after acute social conflict. Mol Neurobiol. 2019;56:3768–79.
36. Shinohara R, Taniguchi M, Ehrlich AT, Yokogawa K, Deguchi Y, Cherasse Y, et al. Dopamine D1 receptor subtype mediates acute stress-induced dendritic growth in excitatory neurons of the medial prefrontal cortex and contributes to suppression of stress susceptibility in mice. Mol Psychiatry. 2018;23:1717–30.
37. Dulka BN, Bourdon AK, Clinard CT, Muvvala MBK, Campagna SR, Cooper MA. Metabolomics reveals distinct neurochemical profiles associated with stress resilience. Neurobiol Stress. 2017;7:103–12.
38. Dulka BN, Bagatelas ED, Bress KS, Grizzell JA, Cannon MK, Whitten CJ, et al. Chemogenetic activation of an infralimbic cortex to basolateral amygdala projection promotes resistance to acute social defeat stress. Sci Rep. 2020;10:6884.
39. Schindelin J, Arganda-Carreras I, Frise E, Kaynig V, Longair M, Pietzsch T, et al. Fiji: an open-source platform for biological-image analysis. Nat Methods. 2012;9:676–82.
40. Du G, Drexler GA, Friedland W, Greubel C, Hable V, Krucken R, et al. Spatial dynamics of DNA damage response protein foci along the ion trajectory of high-LET particles. Radiat Res. 2011;176:706–15.
41. Dumitriu D, Rodriguez A, Morrison JH. High-throughput, detailed, cell-specific neuroanatomy of dendritic spines using microinjection and confocal microscopy. Nat Protoc. 2011;6:1391–411.
42. Barros VN, Mundim M, Galindo LT, Bittencourt S, Porcionatto M, Mello LE. The pattern of c-Fos expression and its refractory period in the brain of rats and monkeys. Front Cell Neurosci. 2015;9:72.
43. Nakakuki T, Birtwistle MR, Saeki Y, Yumoto N, Ide K, Nagashima T, et al. Ligand-specific c-Fos expression emerges from the spatiotemporal control of ErbB network dynamics. Cell.2010;141:884–96.
44. Moench KM, Breach MR, Wellman CL. Chronic stress produces enduring sex- and region-specific alterations in novel stress-induced c-Fos expression. Neurobiol Stress. 2019;10:100147.

45. Kovacs LA, Schiessl JA, Nafz AE, Csernus V, Gaszner B. Both basal and acute restraint stress-induced c-Fos expression is influenced by age in the extended amygdala and brainstem stress centers in male rats. Front Aging Neurosci. 2018;10:248.

46. Conversi D, Orsini C, Cabib S. Distinct patterns of Fos expression induced by systemic amphetamine in the striatal complex of C57BL/6JICo and DBA/2JICo inbred strains of mice. Brain Res. 2004;1025:59–66.

47. Al-Safadi S, Al-Safadi A, Branchaud M, Rutherford S, Dayanandan A, Robinson B, et al. Stress-induced changes in the expression of the clock protein PERIOD1 in the rat limbic forebrain and hypothalamus: role of stress type, time of day, and predictability. PLoS ONE. 2014;9:e111166.

48. Basheer R, Sherin JE, Saper CB, Morgan JI, McCarley RW, Shiromani PJ. Effects of sleep on wake-induced c-fos expression. J Neurosci. 1997;17:9746–50.

49. Francis TC, Chandra R, Friend DM, Finkel E, Dayrit G, Miranda J, et al. Nucleus accumbens medium spiny neuron subtypes mediate depression-related outcomes to social defeat stress. Biol Psychiatry. 2015;77:212–22.

50. Chaudhury D, Walsh JJ, Friedman AK, Juarez B, Ku SM, Koo JW, et al. Rapid regulation of depression-related behaviours by control of midbrain dopamine neurons. Nature.2013;493:532–6.

51. Felix-Ortiz AC, Burgos-Robles A, Bhagat ND, Leppla CA, Tye KM. Bidirectional modulation of anxiety-related and social behaviors by amygdala projections to the medial prefrontal cortex. Neuroscience.2016;321:197–209.

52. Burgos-Robles A, Vidal-Gonzalez I, Quirk GJ. Sustained conditioned responses in prelimbic prefrontal neurons are correlated with fear expression and extinction failure. J Neurosci. 2009;29:8474–82.

53. Bourne J, Harris KM. Do thin spines learn to be mushroom spines that remember? Curr Opin Neurobiol. 2007;17:381–6.

54. Harvey CD, Svoboda K. Locally dynamic synaptic learning rules in pyramidal neuron dendrites. Nature.2007;450:1195–1200.

55. Kasai H, Matsuzaki M, Noguchi J, Yasumatsu N, Nakahara H. Structure-stability-function relationships of dendritic spines. Trends Neurosci. 2003;26:360–8.

56. Matsuzaki M, Ellis-Davies GC, Nemoto T, Miyashita Y, Iino M, Kasai H. Dendritic spine geometry is critical for AMPA receptor expression in hippocampal CA1 pyramidal neurons. Nat Neurosci. 2001;4:1086–92.

57. Matsuzaki M, Honkura N, Ellis-Davies GC, Kasai H. Structural basis of long-term potentiation in single dendritic spines. Nature.2004;429:761–6.

58. Wendelmuth M, Willam M, Todorov H, Radyushkin K, Gerber S, Schweiger S. Dynamic longitudinal behavior in animals exposed to chronic social defeat stress. PLoS ONE. 2020;15:e0235268.

59. Corcoran KA, Quirk GJ. Activity in prelimbic cortex is necessary for the expression of learned, but not innate, fears. J Neurosci. 2007;27:840–4.

60. Milad MR, Quirk GJ. Neurons in medial prefrontal cortex signal memory for fear extinction. Nature.2002;420:70–4.

61. Vidal-Gonzalez I, Vidal-Gonzalez B, Rauch SL, Quirk GJ. Microstimulation reveals opposing influences of prelimbic and infralimbic cortex on the expression of conditioned fear. Learn Mem. 2006;13:728–33.

62. Hultman R, Mague SD, Li Q, Katz BM, Michel N, Lin L, et al. Dysregulation of prefrontal cortex-mediated slow-evolving limbic dynamics drives stress-induced emotional pathology. Neuron.2016;91:439–52.

63. Kumar S, Hultman R, Hughes D, Michel N, Katz BM, Dzirasa K. Prefrontal cortex reactivity underlies trait vulnerability to chronic social defeat stress. Nat Commun. 2014;5:4537.

64. Moda-Sava RN, Murdock MH, Parekh PK, Fetcho RN, Huang BS, Huynh TN, et al. Sustained rescue of prefrontal circuit dysfunction by antidepressant-induced spine formation. Science. 2019;364:1–11.

65. Song C, Ehlers VL, Moyer JR Jr. Trace fear conditioning differentially modulates intrinsic excitability of medial prefrontal cortex-basolateral complex of amygdala projection neurons in infralimbic and prelimbic cortices. J Neurosci. 2015;35:13511–24.

66. Dzirasa K, Kumar S, Sachs BD, Caron MG, Nicolelis MA. Cortical-amygdalar circuit dysfunction in a genetic mouse model of serotonin deficiency. J Neurosci. 2013;33:4505–13.

67. Hultman R, Ulrich K, Sachs BD, Blount C, Carlson DE, Ndubuizu N, et al. Brain-wide electrical spatiotemporal dynamics encode depression vulnerability. Cell.2018;173:166–80 e114.

68. Doyère V, Debiec J, Monfils MH, Schafe GE, LeDoux JE. Synapse-specific reconsolidation of distinct fear memories in the lateral amygdala. Nat Neurosci. 2007;10:414–6.

69. Euston DR, Gruber AJ, McNaughton BL. The role of medial prefrontal cortex in memory and decision making. Neuron.2012;76:1057–70.

70. Gale GD, Anagnostaras SG, Godsil BP, Mitchell S, Nozawa T, Sage JR, et al. Role of the basolateral amygdala in the storage of fear memories across the adult lifetime of rats. J Neurosci. 2004;24:3810–5.

71. Rajasethupathy P, Sankaran S, Marshel JH, Kim CK, Ferenczi E, Lee SY, et al. Projections from neocortex mediate top-down control of memory retrieval. Nature.2015;526:653–9.

72. Veer IM, Oei NY, Spinhoven P, van Buchem MA, Elzinga BM, Rombouts SA. Beyond acute social stress: increased functional connectivity between amygdala and cortical midline structures. Neuroimage.2011;57:1534–41.

73. Wang M, Perova Z, Arenkiel BR, Li B. Synaptic modifications in the medial prefrontal cortex in susceptibility and resilience to stress. J Neurosci. 2014;34:7485–92.

74. Zuo Y, Lin A, Chang P, Gan WB. Development of long-term dendritic spine stability in diverse regions of cerebral cortex. Neuron.2005;46:181–9.

75. Zhou Q, Homma KJ, Poo MM. Shrinkage of dendritic spines associated with long-term depression of hippocampal synapses. Neuron.2004;44:749–57.

76. Kasai H, Fukuda M, Watanabe S, Hayashi-Takagi A, Noguchi J. Structural dynamics of dendritic spines in memory and cognition. Trends Neurosci. 2010;33:121–9.

77. Kasai H, Hayama T, Ishikawa M, Watanabe S, Yagishita S, Noguchi J. Learning rules and persistence of dendritic spines. Eur J Neurosci. 2010;32:241–9.

78. Knott G, Holtmaat A. Dendritic spine plasticity-current understanding from in vivo studies. Brain Res Rev. 2008;58:282–9.

79. Knott GW, Holtmaat A, Wilbrecht L, Welker E, Svoboda K. Spine growth precedes synapse formation in the adult neocortex in vivo. Nat Neurosci. 2006;9:1117–24.

80. Bennett SH, Kirby AJ, Finnerty GT. Rewiring the connectome: evidence and effects. Neurosci Biobehav Rev. 2018;88:51–62.

81. Martin S, Henley JM, Holman D, Zhou M, Wiegert O, van Spronsen M, et al. Corticosterone alters AMPAR mobility and facilitates bidirectional synaptic plasticity. PLoS ONE. 2009;4:e4714.

82. Beltrán-Campos V, Prado-Alcalá RA, León-Jacinto U, Aguilar-Vázquez A, Quirarte GL, Ramírez-Amaya V, et al. Increase of mushroom spine density in CA1 apical dendrites produced by water maze training is prevented by ovariectomy. Brain Res. 2011;1369:119–30.

83. Blair HT, Schafe GE, Bauer EP, Rodrigues SM, LeDoux JE. Synaptic plasticity in the lateral amygdala: a cellular hypothesis of fear conditioning. Learn Mem. 2001;8:229–42.

84. Brown SM, Henning S, Wellman CL. Mild, short-term stress alters dendritic morphology in rat medial prefrontal cortex. Cereb Cortex. 2005;15:1714–22.

85. Butz M, Wörgötter F, van Ooyen A. Activity-dependent structural plasticity. Brain Res Rev. 2009;60:287–305.

86. Engert F, Bonhoeffer T. Dendritic spine changes associated with hippocampal long-term synaptic plasticity. Nature.1999;399:66–70.

87. Fu M, Zuo Y. Experience-dependent structural plasticity in the cortex. Trends Neurosci. 2011;34:177–87.

88. Grutzendler J, Kasthuri N, Gan WB. Long-term dendritic spine stability in the adult cortex. Nature.2002;420:812–6.

89. Hofer SB, Bonhoeffer T. Dendritic spines: the stuff that memories are made of? Curr Biol. 2010;20:R157–159.

90. Sigurdsson T, Doyère V, Cain CK, LeDoux JE. Long-term potentiation in the amygdala: a cellular mechanism of fear learning and memory. Neuropharmacology.2007;52:215–27.

91. Yang Y, Wang XB, Frerking M, Zhou Q. Spine expansion and stabilization associated with long-term potentiation. J Neurosci. 2008;28:5740–51.

92. Holtmaat A, Wilbrecht L, Knott GW, Welker E, Svoboda K. Experience-dependent and cell-type-specific spine growth in the neocortex. Nature.2006;441:979–83.

93. Komatsuzaki Y, Hatanaka Y, Murakami G, Mukai H, Hojo Y, Saito M, et al. Corticosterone induces rapid spinogenesis via synaptic glucocorticoid receptors and kinase networks in hippocampus. PLoS ONE. 2012;7:e34124.

94. Holmes A, Wellman CL. Stress-induced prefrontal reorganization and executive dysfunction in rodents. Neurosci Biobehav Rev. 2009;33:773–83.

95. McEwen BS, Eiland L, Hunter RG, Miller MM. Stress and anxiety: structural plasticity and epigenetic regulation as a consequence of stress. Neuropharmacology.2012;62:3–12.

96. Goldwater DS, Pavlides C, Hunter RG, Bloss EB, Hof PR, McEwen BS, et al. Structural and functional alterations to rat medial prefrontal cortex following chronic restraint stress and recovery. Neuroscience.2009;164:798–808.

97. Liu RJ, Ota KT, Dutheil S, Duman RS, Aghajanian GK. Ketamine strengthens CRF-activated amygdala inputs to basal dendrites in mPFC layer V pyramidal cells in the prelimbic but not infralimbic subregion, a key suppressor of stress responses. Neuropsychopharmacology.2015;40:2066–75.

98. MacLaren DA, Browne RW, Shaw JK, Krishnan Radhakrishnan S, Khare P, Espana RA, et al. Clozapine N-Oxide Administration Produces Behavioral Effects in Long-Evans Rats: Implications for Designing DREADD Experiments. eNeuro. 2016;3:1–14.

99. Padovan-Hernandez Y, Knackstedt LA. Dose-dependent reduction in cocaine-induced locomotion by Clozapine-N-Oxide in rats with a history of cocaine self-administration. Neurosci Lett. 2018;674:132–5.

100. Manvich DF, Webster KA, Foster SL, Farrell MS, Ritchie JC, Porter JH, et al. The DREADD agonist clozapine N-oxide (CNO) is reverse-metabolized to clozapine and produces clozapine-like interoceptive stimulus effects in rats and mice. Sci Rep. 2018;8:3840.

101. Raper J, Morrison RD, Daniels JS, Howell L, Bachevalier J, Wichmann T, et al. Metabolism and distribution of clozapine-N-oxide: implications for nonhuman primate chemogenetics. ACS Chem Neurosci. 2017;8:1570–6.

102. Gomez JL, Bonaventura J, Lesniak W, Mathews WB, Sysa-Shah P, Rodriguez LA, et al. Chemogenetics revealed: DREADD occupancy and activation via converted clozapine. Science.2017;357:503–7.

103. Jiang L, Wu X, Wang S, Chen SH, Zhou H, Wilson B, et al. Clozapine metabolites protect dopaminergic neurons through inhibition of microglial NADPH oxidase. J Neuroinflammation. 2016;13:110.

104. Takahashi A, Chung JR, Zhang S, Zhang H, Grossman Y, Aleyasin H, et al. Establishment of a repeated social defeat stress model in female mice. Sci Rep. 2017;7:12838.

105. Harris AZ, Atsak P, Bretton ZH, Holt ES, Alam R, Morton MP, et al. A novel method for chronic social defeat stress in female mice. Neuropsychopharmacology.2018;43:1276–83.

106. Newman EL, Covington HE 3rd, Suh J, Bicakci MB, Ressler KJ, DeBold JF, et al. Fighting females: neural and behavioral consequences of social defeat stress in female mice. Biol Psychiatry. 2019;86:657–68.

107. Kim MJ, Gee DG, Loucks RA, Davis FC, Whalen PJ. Anxiety dissociates dorsal and ventral medial prefrontal cortex functional connectivity with the amygdala at rest. Cereb Cortex. 2011;21:1667–73.

108. Abend R, Bajaj MA, Harrewijn A, Matsumoto C, Michalska KJ, Necka E, et al. Threat-anticipatory psychophysiological response is enhanced in youth with anxiety disorders and correlates with prefrontal cortex neuroanatomy. J Psychiatry Neurosci. 2021;46:E212–21.

109. Harrewijn A, Kitt ER, Abend R, Matsumoto C, Odriozola P, Winkler AM, et al. Comparing neural correlates of conditioned inhibition between children with and without anxiety disorders - a preliminary study. Behav Brain Res. 2021;399:112994.

110. van Rooij SJH, Smith RD, Stenson AF, Ely TD, Yang X, Tottenham N, et al. Increased activation of the fear neurocircuitry in children exposed to violence. Depress Anxiety. 2020;37:303–12.

111. VanTieghem MR, Tottenham N. Neurobiological programming of early life stress: functional development of amygdala-prefrontal circuitry and vulnerability for stress-related psychopathology. Curr Top Behav Neurosci. 2018;38:117–36.

112. Goetschius LG, Hein TC, Mattson WI, Lopez-Duran N, Dotterer HL, Welsh RC, et al. Amygdala-prefrontal cortex white matter tracts are widespread, variable and implicated in amygdala modulation in adolescents. Neuroimage.2019;191:278–91.

113. Thai M, Schreiner MW, Mueller BA, Cullen KR, Klimes-Dougan B. Coordination between frontolimbic resting state connectivity and hypothalamic-pituitary-adrenal axis functioning in adolescents with and without depression. Psychoneuroendocrinology.2021;125:105123.

114. Swaab DF, Bao AM. Sex differences in stress-related disorders: major depressive disorder, bipolar disorder, and posttraumatic stress disorder. Handb Clin Neurol. 2020;175:335–58.

115. Ginty AT, Kraynak TE, Kuan DC, Gianaros PJ. Ventromedial prefrontal cortex connectivity during and after psychological stress in women. Psychophysiology.2019;56:e13445.

116. Hanson JL, Albert WD, Skinner AT, Shen SH, Dodge KA, Lansford JE. Resting state coupling between the amygdala and ventromedial prefrontal cortex is related to household income in childhood and indexes future psychological vulnerability to stress. Dev Psychopathol. 2019;31:1053–66.

ACKNOWLEDGEMENTS

AUTHOR CONTRIBUTIONS
YSG, CF, PJK and DD designed experiments, YSG, CF, AM, RW, TZ, GV, WGJ and DD performed experiments, YSG, CF, TZ and DD analyzed the data. YSG, AM and DD wrote the paper. All authors read and approved the paper.

FUNDING

COMPETING INTERESTS
The authors declare no competing interests.

ADDITIONAL INFORMATION
Supplementary information The online version contains supplementary material available at https://doi.org/10.1038/s41386-021-01229-6.

Correspondence and requests for materials should be addressed to Dani Dumitriu.

Reprints and permission information is available at http://www.nature.com/reprints